Performance characterization of a novel thin position-sensitive avalanche photodiode-based detector for high resolution PET

Jin Zhang, *Member, IEEE* Angela M K Foudray, *Student Member, IEEE,* Peter D Olcott, *Member, IEEE* and Craig S Levin, *Member, IEEE*

***Abstract*— We are developing advanced dedicated breast and small animal positron emission tomography (PET) systems with detectors comprising arrays of 1x1x3 mm^3 LSO crystals coupled to novel, extremely thin position-sensitive avalanche photodiodes (PSAPD). This thin PSAPD is essential for achieving high crystal packing fraction for a PET system design which has 2 cm effective LSO crystal thickness, 1mm transaxial spatial resolution and 3 mm directly measured photon DOI resolution. These properties facilitate high detection efficiency and three dimensional positioning capability in the detector. With this very thin PSAPD, preliminary results indicated that we can expect 1 mm^3 intrinsic spatial resolution. We have observed an average of 1.1mm transaxial and 3mm DOI spatial resolution, ∼11% energy resolution and ∼2 ns temporal resolution. We have also implemented a position algorithm for reducing the effect of pincushioning on events detected over the face of the PSAPD.**

***Index Terms*— Position Sensitive Avalanche Photodiode, PSAPD, Positron Emission Tomography, Energy Resolution, Coincidence Time Resolution, Position Resolution, Position Algorithm**

I. Introduction

SEMICONDUCTOR based detectors have been a promising choice for dedicated ultra-high resolution positron emission tomography (PET) systems. A novel silicon based position-sensitive avalanche photodiode (PSAPD) [1] packaged on ceramic substrate has been tested with LSO scintillation crystals and good energy (12.29±0.46% at 511 keV, on whole active area) and time resolutions (2.15±0.35 ns) were achieved [2]. However, in order to have edge-on geometry of the PET camera as proposed by Levin et al [3], an ultra-thin PSAPD (<300 μm) is required in order to achieve high packing fraction. For this purpose, new PSAPDs with the silicon chip (∼180-250 μm) mounted on a 50μm thick polyimid flex circuit were fabricated. The objective of this study is to measure energy, coincidence time and spatial resolutions of this thin PSAPD and compare results to those achieved with the ceramic packaged devices. In this paper, we present experimental results on the energy resolution (ER), coincidence time resolution (CTR) and spatial resolution (SR) performance of the standard (ceramic substrate) and thin flex PSAPDs.

Manuscript received November 11, 2005. This work was supported in part by NIH-NCI grant R21 CA098691 and NIH-NIBIB grant R21 EB003283.

Jin Zhang (jin.zhang@perkinelmer.com) was with the Department of Radiology, the Molecular Imaging Program at Stanford University. He is now with PerkinElmer Optoelectronics, Santa Clara, CA 95054. Angela M.K. Foudray (afoudray@stanford.edu), Peter D. Olcott (pdo@stanford.edu) and Craig S. Levin (cslevin@stanford.edu) are with the Department of Radiology and the Molecular Imaging Program, Stanford University, Stanford, CA 94305. AMKFoudray is also with the Department of Physics, University of California, San Diego.

II. Materials and Methods

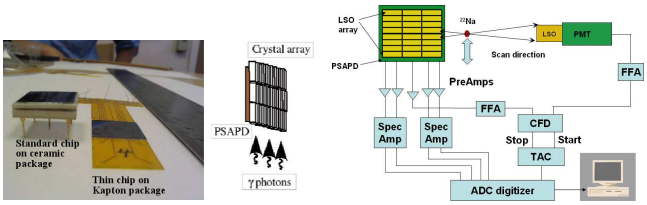

(a) (b)

Fig. 1. Picture and data acquisition setup of the PSAPD characterized. (a) Picture of PSAPD with standard package and thin Kapton flex cable package, and edge-on crystal configuration for directly measured photon interaction depth, high detection efficiency and ¿90% light collection efficiency. (b) Schematic of experimental setup for coincidence point spread function and coincidence time resolution experimental measurements.

The detectors are based on arrays of lutetium oxyorthosilicate (LSO) crystals (1x1x3 mm^3) coupled to new 11x11 mm^2 position sensitive avalanche photodiodes (PSAPD) with a sensitive area of 8x8 mm^2 and thickness of < 0.3 mm, to be used edge-on with respect to incoming photons (figure 1a). The typical experimental setup for coincidence measurements is shown in figure 1b.

Flood images were generated using data from the four corner signals of the PSAPD. Previously, Anger-type logic was used for the 2-D positioning calculation, which can be expressed as:

$$X = \frac{(A+B)-(C+D)}{A+B+C+D} \quad (1)$$

$$Y = \frac{(A+D)-(B+C)}{A+B+C+D} \quad (2)$$

where A, B, C, and D are signals from the four channels of the PSAPD; X and Y are the coordinate of the photon interaction position on the detector surface. However, using

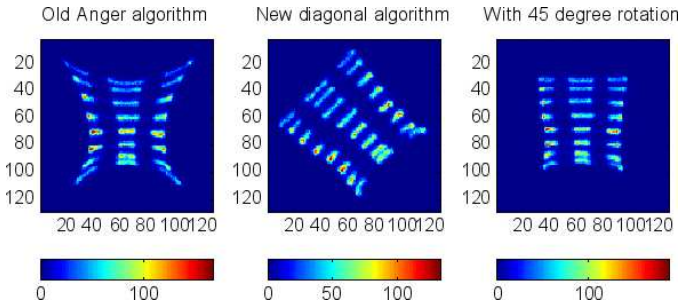

Fig. 2. Flood images generated by the Anger-like algorithm (left) and our new algorithm (middle and right) with a 8x3 array of LSO crystals with the new thin PSAPD.

Anger-type logic, flood images always show significant pincushion distortion due to the non-linearity of the device (figure 2a).

We have developed another Anger-like algorithm that uses only two diagonal channels at a time to determine the position of gamma photon interaction, which can be expressed as:

$$X' = \frac{A - C}{A + C} \tag{3}$$

$$Y' = \frac{B - D}{B + D} \tag{4}$$

$$X = X'cos(\frac{\pi}{4}) + Y'sin(\frac{\pi}{4}) \tag{5}$$

$$Y = Y'cos(\frac{\pi}{4}) - X'sin(\frac{\pi}{4}) \tag{6}$$

As diagonal channels are used to determine X and Y, we need to rotate the image by π/4 to reorient the image to the XY coordinate system. The advantage of this algorithm is that it generates flood images with significantly reduced pincushion distortion and thus will be used in this paper for analysis of the PSAPD performance.

III. Results

A. Energy Resolution with 4x3 and 8x3 Arrays

Energy resolution for both the larger 2x2x3mm^3 crystals in the 4x3 array and the 8x3 array of 1x1x3mm^3 crystals was measured by position gating events from a flood measurement. Flood measurements were made with a 500μm ^{22}Na source for both the standard ceramic PSAPD and the thin PSAPD. Two dimensional histograms from the flood measurement are shown for the crystal arrays coupled side-on to the PSAPD devices (with an 8x8 mm^2 sensitive area). The crystal locations are segmented from the flood images from which individual crystal energy spectra are extracted.

For the data shown in figure 3, each crystal has a size of 2x2x3 mm^3. The left hand side of the data are for the standard ceramic device. The individual crystal average photopeak position for the twelve crystals is 3.64$\pm$0.01 volts (figure 3b top). The average photon counts in the FWHM of the photopeak are 5267$\pm$108 photons (figure 3b middle). The average crystal ER at 511 keV is 10.85$\pm$0.62% (figure 3b bottom), the best ER is 9.95$\pm$0.51% (figure 4 left) and the worst ER is 11.76$\pm$0.73%.

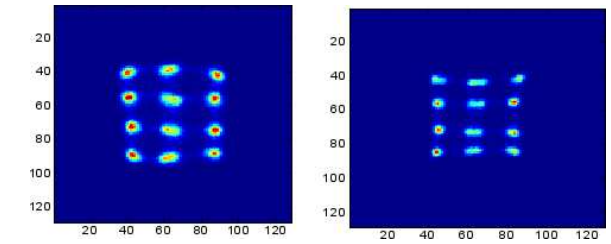

(a) Flood images.

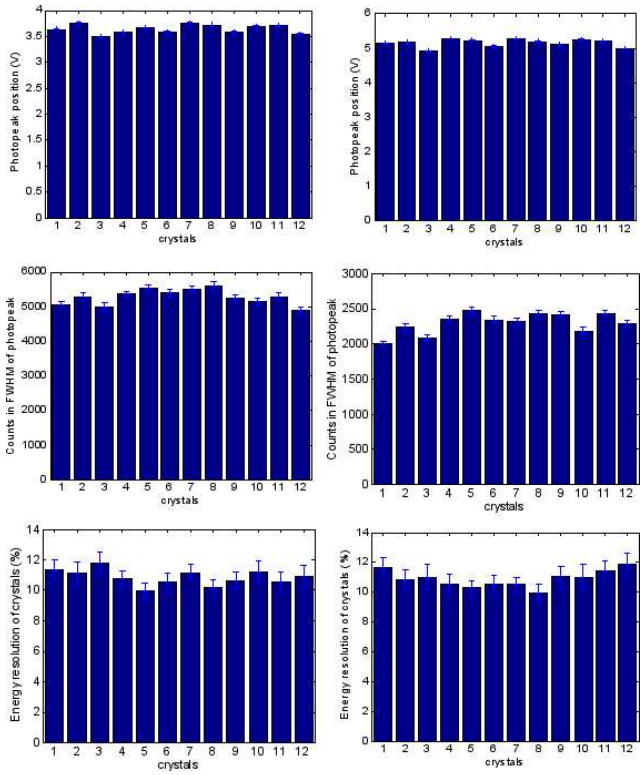

(b) (top) bar plot of photopeak position; (middle) bar plot of counts in FWHM; and (bottom) bar plot of photopeak energy resolution for individual crystals.

Fig. 3. Flood histogram data for the 4x3 array of 2x2x3mm^3 LSO crystals coupled to standard PSAPD (left) and novel thin PSAPD (right).

For the thin flex circuit PSAPD, as shown in the right hand side of figure 3, the crystals average photopeak position for the twelve crystals was 5.14$\pm$0.01 volts (figure 3b top). The source was placed further from the PSAPD in this experiment than with the ceramic device, therefore the average photon counts in the FWHM of the photopeak were 2293$\pm$49.5 photons (figure 3b middle). The average ER at 511keV for the 12 crystals was 10.89$\pm$0.66% (figure 3b bottom) with the best ER of 9.94$\pm$0.59% (figure 4 right) and the worst ER of 11.88$\pm$0.7%. The crystals appear smaller and better separated for the thin device.

We also compared the ER with both detectors coupled with a 8x3 LSO array of 1x1x3 mm^3 crystals. There were no inter-crystal reflectors or gaps. Thus the array covers a total area of

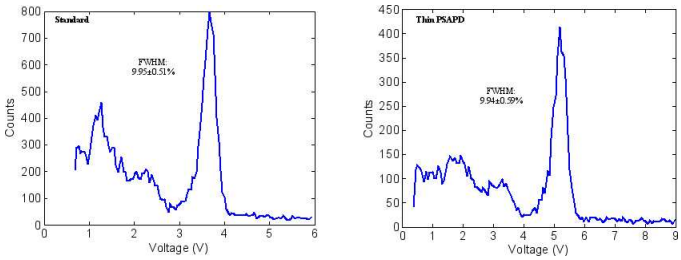

Fig. 4. Best energy resolution spectra of standard (left) and new thin (right) PSAPD.

8x9 mm^2, which is slightly bigger than the actual 8x8 mm^2 active area of each PSAPD. In order to compare the effect of crystals surface finish on the performance, half crystals used are with ground or as-cut surface and another half crystals with polished surface. Figure 5 shows the comparison of the flood images with photopeak position, photon counts in FWHM and energy resolutions of each crystal. For the standard PSAPD (figure 5 left), the crystals average photopeak position for the 24 crystals is 4.33±0.02 volts (figure 5b top). The average photon counts in the FWHM of the photopeak are 2873±78.6 photons (figure 5b middle). The average ER at 511keV for the 24 crystals is 12.61±0.97% (figure 5b bottom), with the best ER of 10.8±0.77% and the worst ER of 14.49±1.5%.

On the other hand, for the new thin PSAPD (right hand side figures), the crystals average photopeak position for the 24 crystals is 5.71±0.03 volts (figure 5b top). The average photon counts in the FWHM of the photopeak are 1604±53.8 photons (figure 5b middle). The average ER at 511keV for the 24 crystals is 12.88±1.2% (figure 5b bottom), with the best ER of 10.0±0.86% and the worst ER of 17.36±1.7%.

B. Temporal Resolution and Spatial Resolution

CTR was also measured for both PSAPDs. A small LSO crystal coupled to a PMT was used as the start channel to the TAC and signals from the sum energy channel of the PSAPD was used as the stop channel to the TAC. Figure 6 shows that the measured CTR of standard (left) and thin devices (right), with FWHM energy gating, is 2.01±0.22 ns and 1.97±0.25 ns, respectively.

In the measurement of the coincidence SR, the same LSO crystal coupled to a PMT used for the CTR measurement was mounted rigidly on a motor-driven stage with a 10 μCi ^{22}Na source. Then this stage was scanned along the edge of the 8x3 LSO crystal array along the 8 crystal edges with a 511 keV photon beam size of about 0.6 μm. Each crystal has a size of 1x1x3 mm^3 and there were no inter-crystal reflectors or gaps. Thus the array covers a total area of 8x9 mm^2, which is slightly bigger than the actual 8x8 mm^2 active area of each PSAPD. Again, to evaluate the performance of different crystal surface finish, the 8x3 LSO array contains 12 crystals with polished surface on all side, and another 12 crystals with all ground surface.

The sum of raw scanning data in figure 7 shows that the polished crystals have higher light output than the ground crystals. Notice that the left two columns of crystals (polished) are not clearly resolved by the standard PSAPD (figure 7). However,

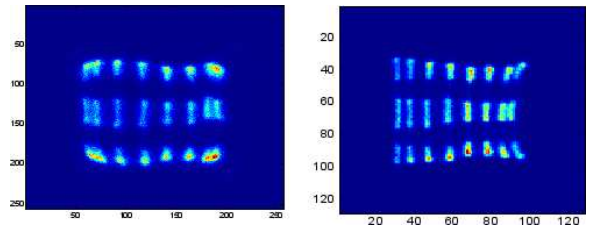

(a) Flood images.

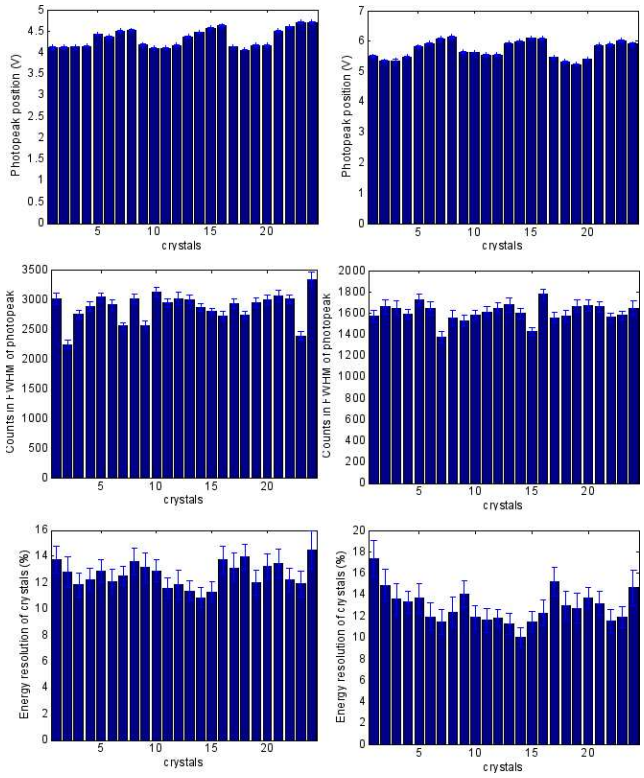

(b) (top) bar plot of photopeak position; (middle) bar plot of counts in FWHM; and (bottom) bar plot of photopeak energy resolution for individual crystals.

Fig. 5. Flood histogram data for the 8x3 array of 1x1x3mm^3 LSO crystals coupled to standard PSAPD (left) and novel thin PSAPD (right).

the new flex PSAPD clearly resolved the entire 3x8 crystal array in the sum image. Analysis showed the polished crystals also have better average ER of 12.5±1.2% vs 14.7±1.3% for ground crystals. The point spread functions (PSF) of the eight crystals closest to the scanning source (bottom eight crystals in each raw sum image) are also shown in figure 7. The average FWHM of raw PSFs for the standard and flex PSAPD is 1.25±0.1 mm and 1.29±0.09 mm, respectively. With photon beam size deconvolution, the intrinsic SR is 1.09±0.1 mm and 1.14±0.09 mm, for the standard and thin PSAPD respectively.

We also did the spatial scan experiment along the 3mm side of the polished and ground crystals. Figure 8 shows the point spread functions of the three polished or ground crystals along the 3mm side. For the standard PSAPD, the

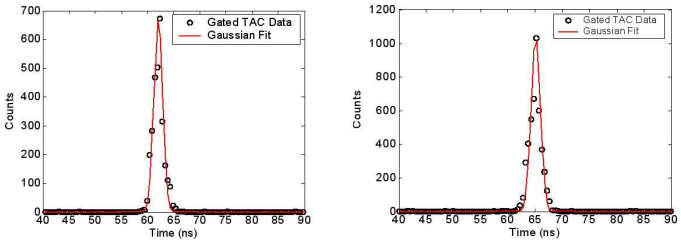

Fig. 6. Coincidence time resolution of the standard PSAPD (left) and thin PSAPD (right).

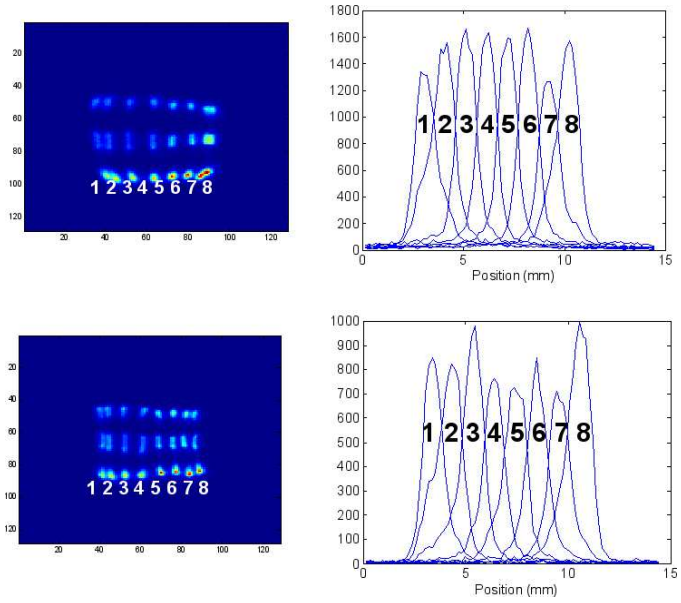

Fig. 7. Spatial resolution (coincidence point spread function) results of standard PSAPD (top) and thin PSAPD (bottom). Left: Sum of raw data collected for point spread function measurements. Right: Point spread functions of the bottom 8 crystals in flood images, which are closest to the scanning source.

average FWHM of the point spread functions for the ground and polished crystals is 3.08±0.04 mm and 2.96±0.05 mm, respectively. For the new thin PSAPD, the average FWHM of the point spread functions for the ground and polished crystals is 3.03±0.05 mm and 2.97±0.07 mm, respectively. The difference in CSR for the ground and polished crystals are due to the smaller size of polished crystals. For both detectors, the CSR is comparable.

IV. Discussion

Our goal was to develop ultra-high resolution PET cameras with high detection efficiency and directly measured DOI resolution. In order to achieve ultra-high spatial resolution, we used a 1x1x3mm^3 LSO crystal array with 3mm DOI resolution inherent in the design. We previously evaluated the standard PSAPD for device performance for PET camera designs and found it to be a viable, high performance photodetector [2]. Having significantly changed certain aspects of the PSAPD design, we assessed the novel thin flex-mounted PSAPD performance to ensure that it worked as expected. All performance characteristics studied for the thin PSAPD were either comparable or superior to the standard device.

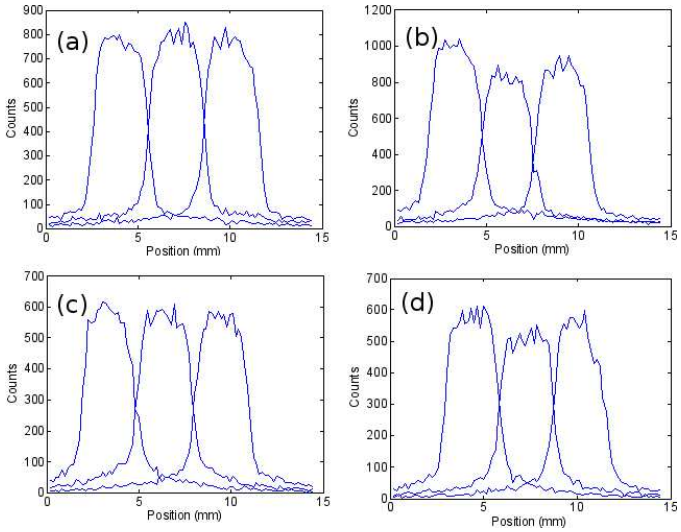

Fig. 8. Spatial resolution of standard PSAPD along the 3mm (depth) dimension of (a) ground and (b) polished LSO crystals, and of thin flex PSAPD for (c) ground and (d) polished crystals.

The good energy and coincidence time values are very important for PET cameras to achieve high contrast resolution. With the ∼12% FWHM energy resolution and ∼2ns FWHM time resolution obtained with the new PSAPD, one can use narrower energy and coincidence time gates to significantly reduce the random and scatter coincidence event rates and improve the signal-to-noise ratio and consequently, the image quality and quantitative accuracy. For example, with this thin PSAPD, we can use 2-4 ns time window and 12-24% energy window for data collection while maintaining high counting statistics.

Most PET detector research has tried to push the limit of spatial resolution to around 2 mm [4]–[6]. Using 1x1x3mm^3 LSO crystals coupled to novel thin PSAPDs, we observed an intrinsic spatial resolution of about 1.1 mm and a DOI resolution of about 3 mm. These resolution values are crucial to improve the visualization capability of the PET camera. We have used Monte Carlo simulation to evaluate systems with different crystal resolutions and we found that the 1x1x3 mm^3 crystal PET systems have superior spatial resolution and contrast than PET systems based on 2x2x10mm^3, 3x3x30mm^3 and 4x4x20mm^3 LSO crystals [7].

V. Conclusion

The recently developed, thin, polyimid flex circuit mounted PSAPD has comparable energy and time resolutions to the ceramic packaged standard PSAPD, and it also generates ∼40% higher photopeak pulse height. The new thin PSAPD also shows better crystal identication ability. This extremely thin PSAPD is essential for achieving high crystal packing fraction for a PET system design [7], [8] with 1 mm^3 intrinsic spatial, <12% FWHM energy resolution, and 2 ns FWHM temporal resolution, 2 cm effective LSO crystal thickness, and 3 mm directly measured photon DOI resolution. In summary, the new PSAPD-based detector achieves the design specifications for the proposed ultra-high resolution PET systems.

ACKNOWLEDGMENT

This work was supported in part by NIH-National Cancer Institute (R21 CA098691) and NIH-NIBIB (R21 EB003283).

REFERENCES

[1] K. S. Shah, R. Farrell, R. Grazioso, E. S. Harmon, and E. Karplus, "Position-sensitive avalanche photodiodes for gamma-ray imaging," *IEEE Trans Nucl Sci*, vol. 49, no. 4, pp. 1687 – 1692, Aug 2002, part 1.

[2] C. S. Levin, A. M. K. Foudray, P. D. Olcott, and F. Habte, "Investigation of position sensitive avalanche photodiodes for a new high resolution pet detector design," *IEEE Nucl Sci Symp Conf Rec*, vol. 4, pp. 2262 – 2266, Oct 2003.

[3] C. S. Levin, "Design of a high-resolution and high-sensitivity scintillation crystal array for pet with nearly complete light collection," *IEEE Trans Nucl Sci*, vol. 49, no. 5, pp. 2236 – 2243, Oct 2002, part 1.

[4] J. Qi, C. Kuo, R. H. Huesman, G. J. Klein, W. M. Moses, and B. W. Reutter, "Comparison of rectangular and dual-planar positron emission mammography scanners," *IEEE Trans. Nucl. Sci*, vol. 49, pp. 2089–2096, 2002.

[5] N. K. Doshi, Y. Shao, R. W. Silverman, and S. R. Cherry, "Design and evaluation of an lso pet detector for breast cancer imaging," *Med. Phys.*, vol. 27, no. 7, pp. 1535–1543, 2000.

[6] Y. C. Tai, A. F. Chatziioannou, Y. Yang, R. W. Silverman, K. Meadors, S. Siegel, D. F. Newport, J. R. Stickel, and S. R. Cherry, "Micropet ii: design, development and initial performance of an improved micropet scanner for small-animal imaging," *Phys. Med. Biol.*, vol. 48, no. 11, pp. 1519–1537, 2003.

[7] J. Zhang, P. D. Olcott, A. M. K. Foudray, G. Chinn, and C. S. Levin, "Monte carlo simulation study of a dual-plate pet camera dedicated to breast cancer imaging," *IEEE Trans Nucl Sci*, 2005, submitted.

[8] A. M. K. Foudray, F. Habte, G. Chinn, J. Zhang, and C. S. Levin, "Optimization of a pet imaging system with direct depth of interaction measurement comprised of position sensitive avalanche photodiodes utilizing monte carlo simulation," *in preparation*, 2006.